ISCI, Volume *9*

Supplemental Information

Low-Frequency Spike-Field Coherence Is a Fingerprint of Periodicity Coding in the Auditory Cortex

Francisco García-Rosales, Lisa M. Martin, M. Jerome Beetz, Yuranny Cabral-Calderin, Manfred Kössl, and Julio C. Hechavarria

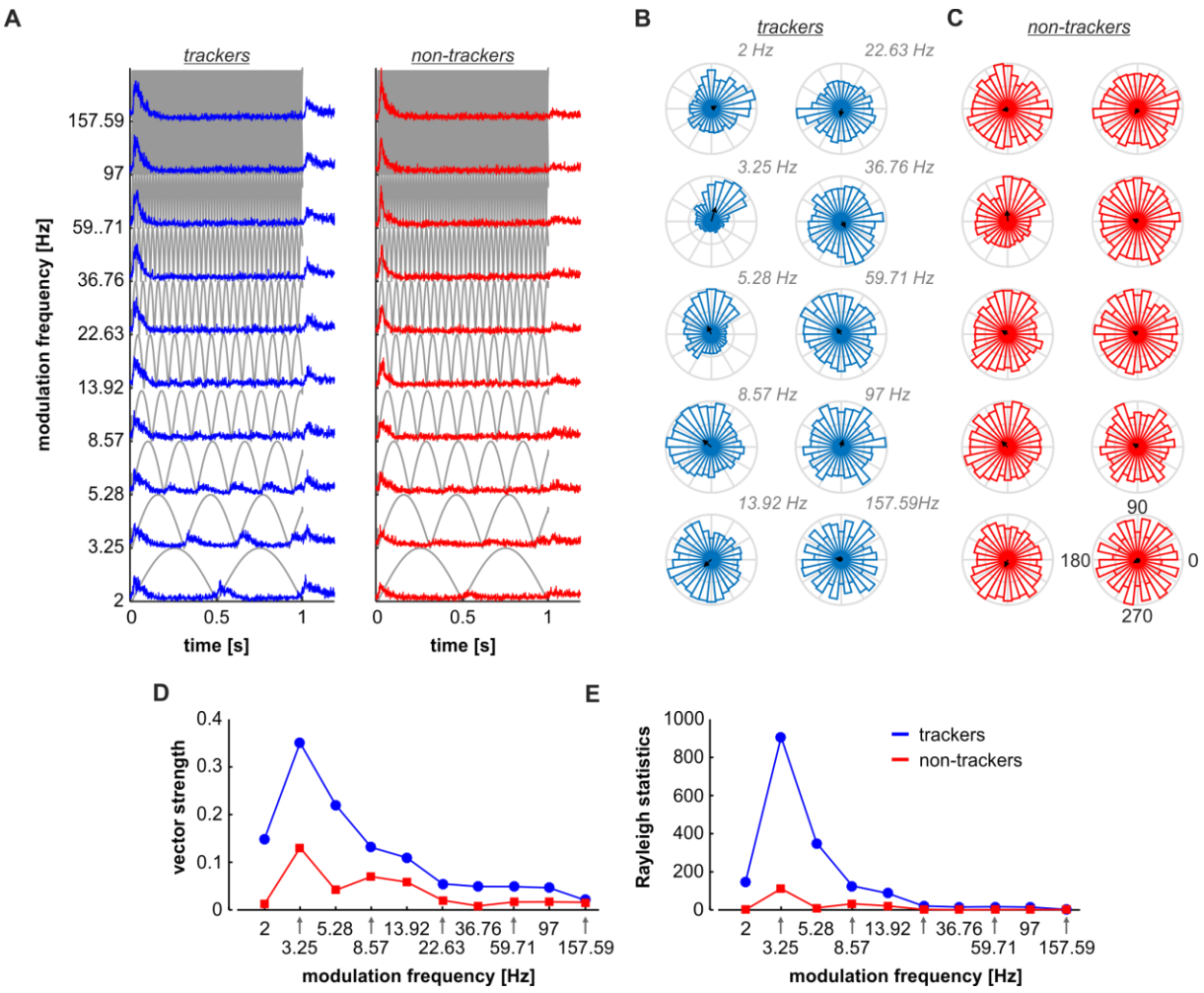

Fig. S1. Pooled responses reveal weak temporal organization for non-tracking units (related to Figure 1). (**A**) Normalized peri-stimulus time histograms (PSTH) calculated from the pooled activity of tracking (blue, left) and non-tracking (red, right) units, in response to all modulation frequencies tested. (**B**) Distribution of spike-phases relative to the AM envelopes, across modulation frequencies, for the pooled spiking of tracking units. Circular histograms show that spike-phases are well-grouped up to modulation rates of 22.63 Hz, suggesting that units fire at similar phases in response to the same modulation frequency. Black arrows represent the mean vector for the phase distribution. (**C**) Spike-phases relative to the AM envelope, across modulation rates, for the pooled spiking of non-tracking units. A weak but still visible clustering of the spike-phases occurs in response to modulation frequencies < 22.63 Hz, particularly at AM rates of 3.25 and 8.57 Hz. (**D**) Vector strength (VS) calculated for the pooled spiking of tracking (blue) and non-tracking (red) units. (**E**) Rayleigh statistics of the spike-phases for pooled tracking (blue) and non-tracking (red) units.

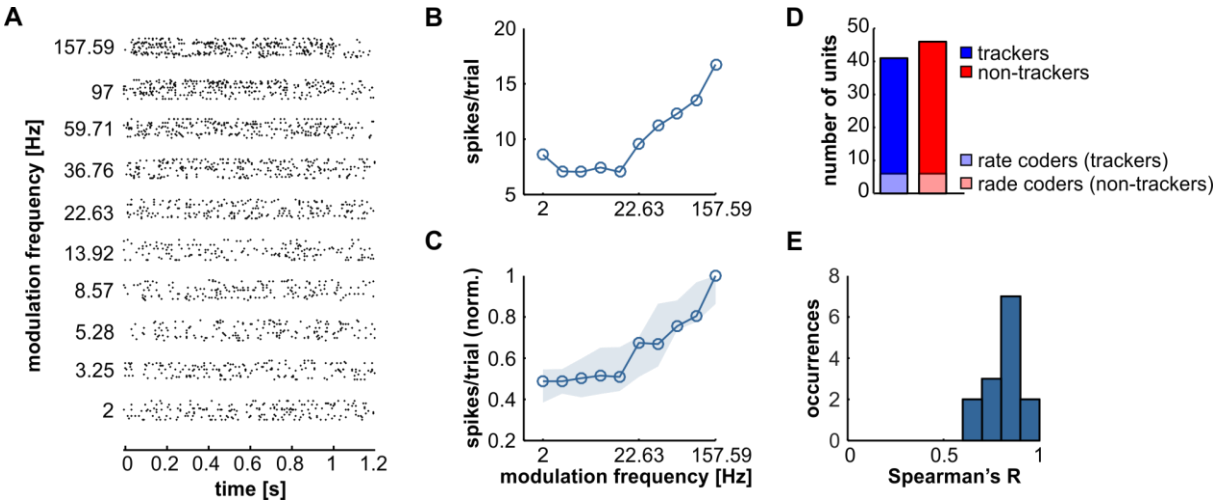

Fig. S2. Rate coding in the auditory cortex of *Carollia perspicillata* (related to Figure 1). (**A**) Scatter plot of an exemplary rate coding unit. For the rate coding analyses, spikes were considered in the period from 0 to 1 s (i.e. the time window of the stimulus) (**B**) Spiking rate (spikes/trial), for each modulation rate, of the example unit shown in **A**. Note the monotonic increase of the firing rate relative to the modulation rate. The Spearman's R of this unit (i.e. the correlation between spiking rate and modulation frequency) was of 0.81 ($p = 4.6x10^{-3}$). (**C**) Normalized spiking rate across the population of rate coding units (n = 12). Note that the firing rate increases with modulation frequencies, particularly in response to periodicities higher than 13.92 Hz. (**D**) Quantification of rate coding units in the groups of trackers (blue) and non-trackers (red). (**E**) Spearman's R of the population of rate coders. High values indicate a strong correlation between firing rate and modulation frequency.

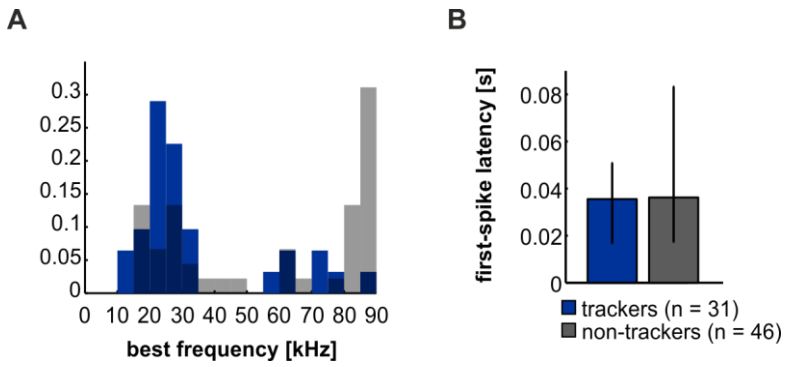

Fig. S3. **Basic properties of tracking and non-tracking units (related to Figures 1 and 3).** (**A**) Distribution of best frequencies (BF, tone frequency at which a unit responded with the most spikes) of tracking (blue histogram) and non-tracking (gray histogram) units. There were significant differences in the BF distribution of trackers and non-trackers (two-sample Kolmogorov-Smirnov test, $p = 0.0019$). (**B**) First spike latency of tracking (blue) and non-tracking (gray; shown as median and quartiles in both cases) units in response to AM stimuli (first spike times were pooled across modulation frequencies). There were no significant differences between the two subpopulations (FDR-corrected Wilcoxon ranksum test, $p = 0.2941$).

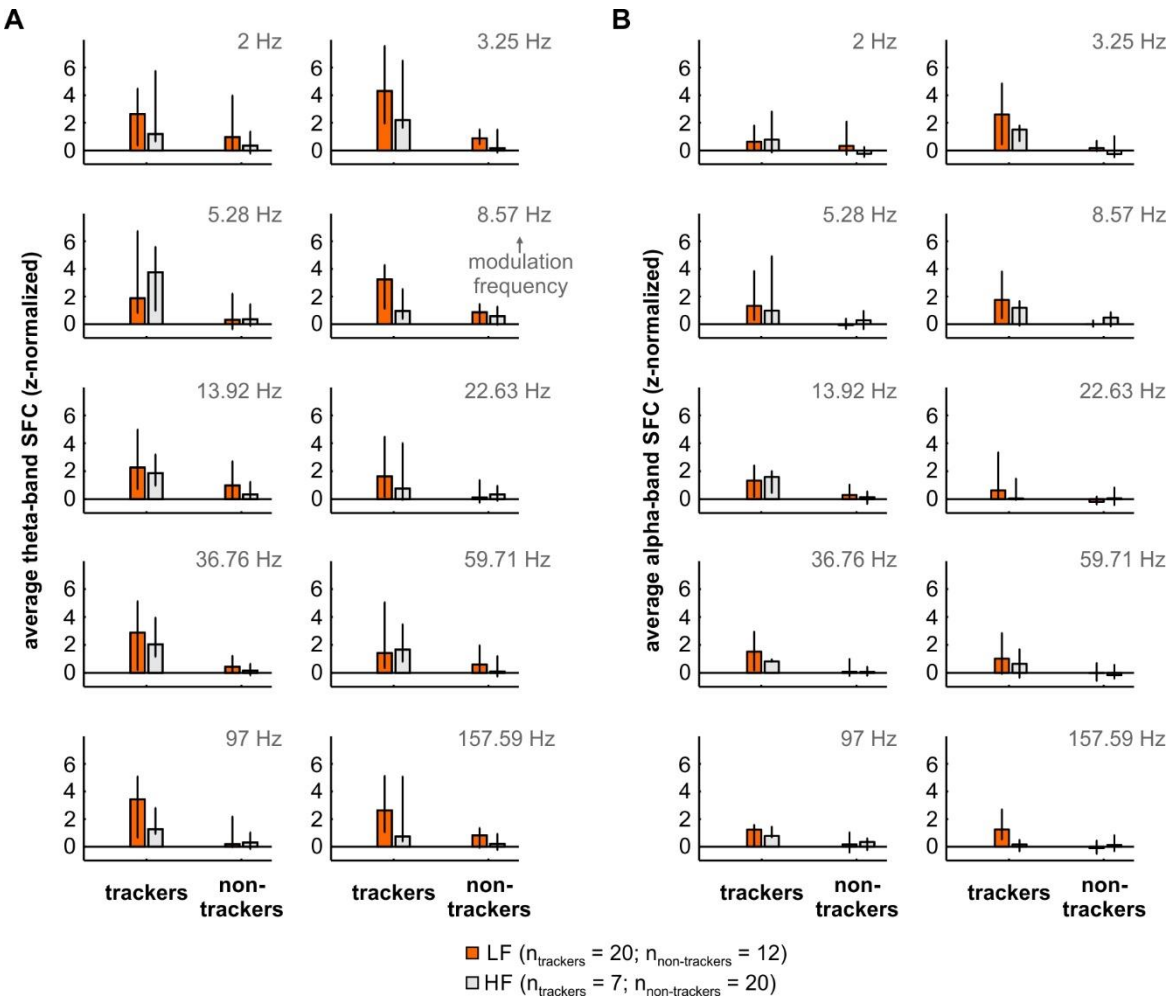

Fig. S4. Spike-field coherence was not significantly different between low and high frequency units (related to Figures 3 and S3). (**A**) Each sub-panel shows the comparison of theta-band z-normalized SFC between low (orange) and high (gray) frequency units within the subpopulation of trackers or non-trackers (left set, or right set, respectively), across modulation rates. Units were deemed as low frequency tuned if their best-frequency was not higher than 50 kHz, and high frequency tuned otherwise, as in previous articles (Esser and Eiermann, 1999; Hagemann et al., 2010; Hagemann et al., 2011). (**B**) Data is shown following the same conventions as in (**A**), but SFC values were compared in the alpha-band (8 – 12 Hz). There were no significant differences in the spike-field coherence of low and high frequency tuned neurons in theta- and alpha-bands (FDR-corrected Wilcoxon ranksum test; corrected $p > 0.066$). The data is shown as median and IQR. Sample sizes are indicated in the figure.

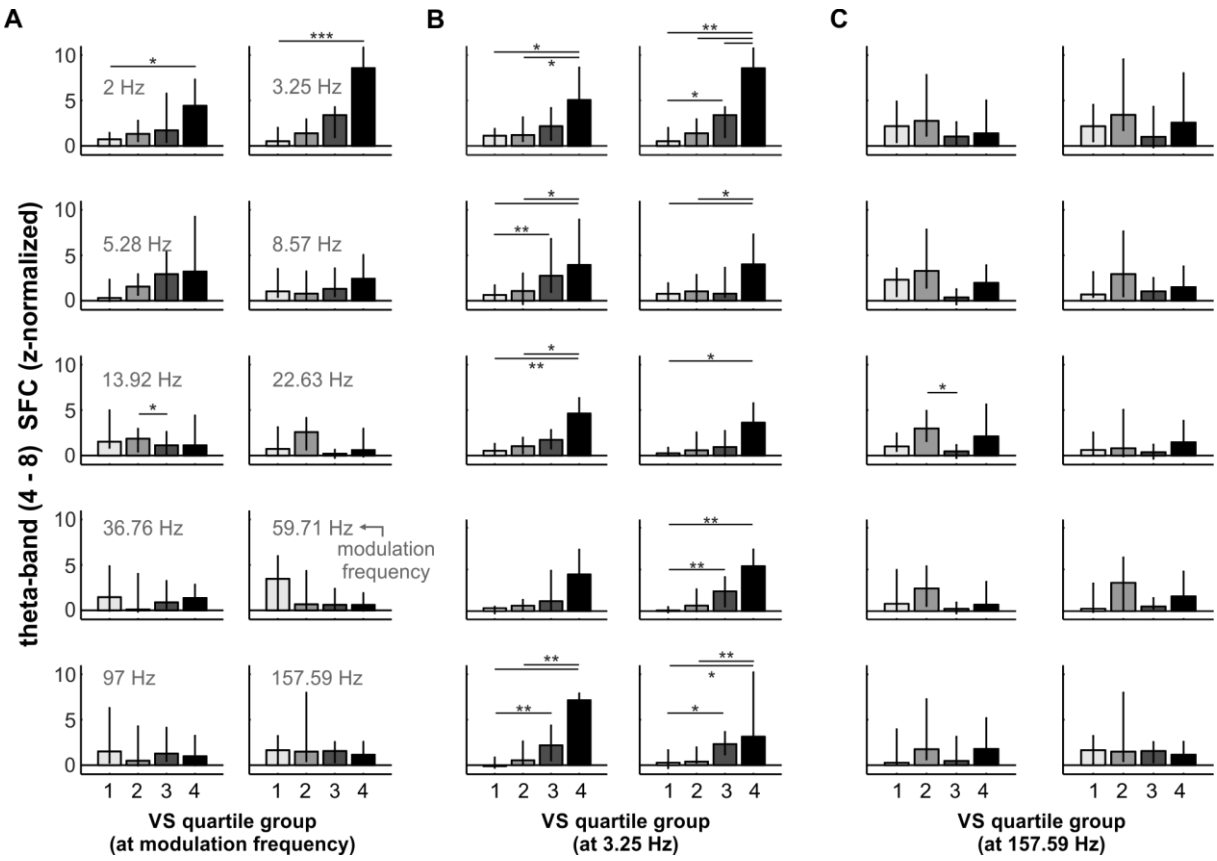

Fig. S5. Theta-band SFC is related to the strength of spike-stimulus synchronization (related to Figure 3). (**A**) Subsets of SFC values across units, divided according to the VS at the modulation frequency under consideration (note that there are four equipopulated subsets, each of n = 17 units; modulation rates are indicated in the plots). VS quartile group 1 contains units with the lowest 25 % vector strength values, whereas group 4 contains units with the highest 25 % vector strength values. The SFC increases together with the VS quartile group, provided that spike-AM synchronization strength is calculated in response to modulation rates < 13.92 Hz. (**B**) Relationship of theta-band spike field coherence, dividing the units into VS quartiles considering spike-stimulus synchronization in response to a modulation rate of 3.25 Hz. Across modulation frequencies, SFC values increased together with VS quartile group. (**C**) Same as in **A** and **B**, but VS values considered were obtained in response to a modulation frequency of 157.59 Hz. Note that there is no relationship between SFC values and VS quartile groups. (significance was assessed with FDR-corrected Wilcoxon rank-sum tests; *, corrected $p < 0.05$; **, corrected $p < 0.01$).

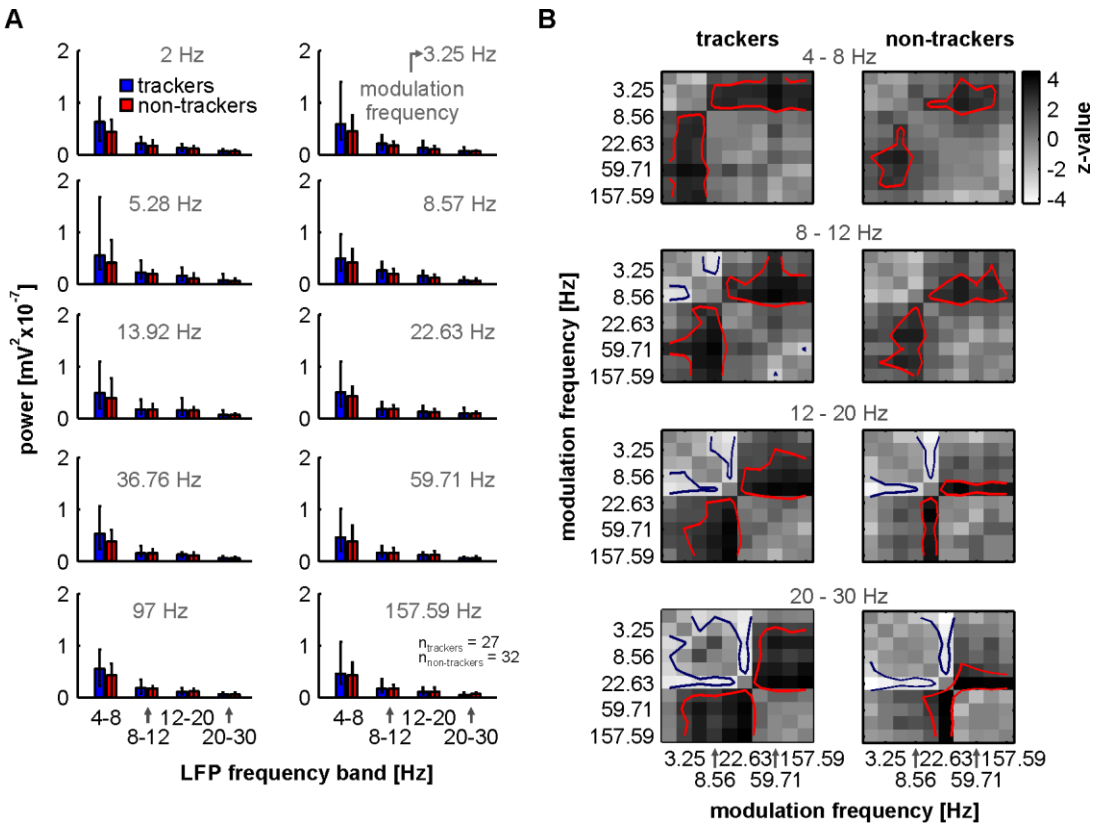

Fig. S6. Power in low frequency bands of the LFP does not explain differences in spike-field coherence (related to Figure 4). (**A**) LFP power in the canonical low frequency bands analyzed in the study, shown for trackers (blue) and non-trackers (red), across modulation frequencies. There were no significant differences in the power of the LFP related to trackers and non-trackers, in any frequency band analyzed (FDR-corrected Wilcoxon ranksum test, $p > 0.06$). (**B**) Each matrix depicts the outcome (z-value) of statistical pairwise comparisons (Wilcoxon signed ranked tests), comparing the power in the LFP of trackers (left column) or non-trackers (right column) in response to each modulation rate. For example, the top-left matrix shows pairwise comparisons of theta-band LFP power (from tracking units) in response to different modulation rates. The value of each cell (i,j) in the matrix is the z statistic obtained by comparing the LFP power in response to modulation frequencies i and j. Red and blue contour lines limit regions of statistical significance (red, power in response to modulation rate i was higher than the power in response to modulation rate j; blue indicates the opposite). The significance threshold was of z = +-2.33 (equivalent to an FDR-corrected p = 0.0198). In the top-matrix it can be observed that the power of theta band LFPs, in trackers, was significantly higher in response to a modulation rate of 3.25 Hz, than in response to modulation rates > 8.56 Hz. Note that, overall, in each neuronal group there were significant differences in the LFP power in response to distinct modulation rates, which also depended on the frequency band under consideration.

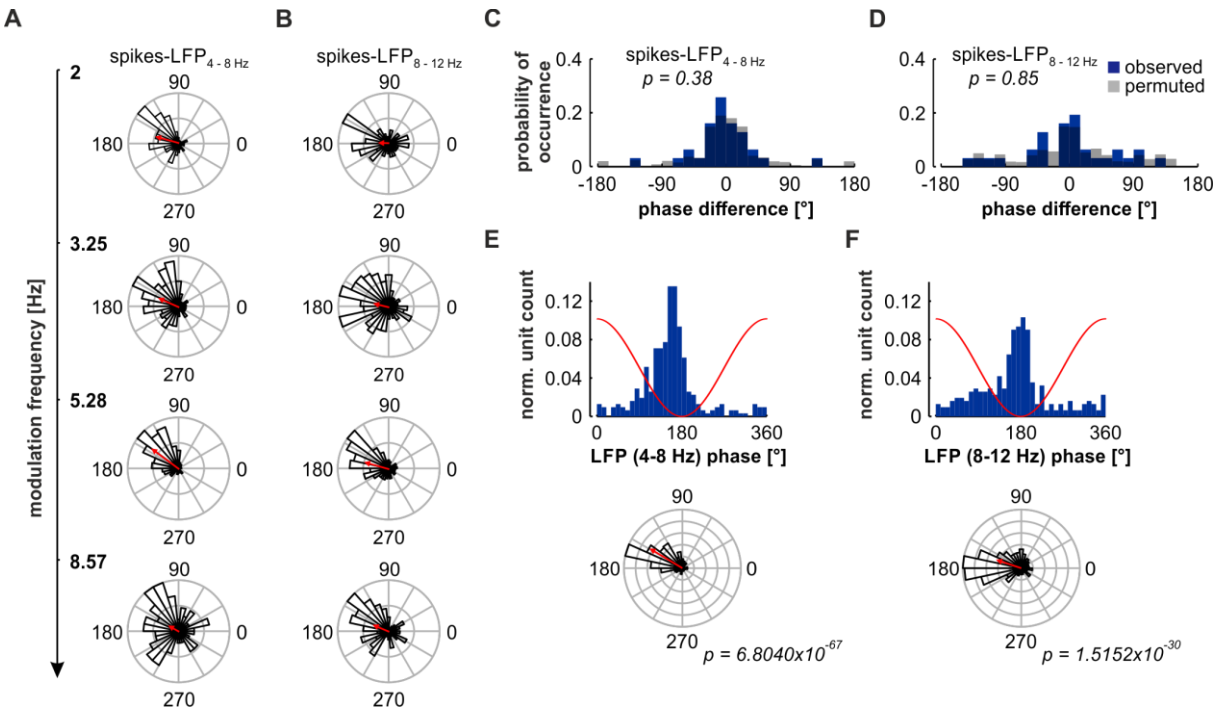

Fig. S7. Robustness of spike-phases relative to theta and alpha bands of the LFP across modulation rates (related to Figure 6). (**A**) *Left column*: spike-phases relative to theta (4 - 8 Hz) band LFPs, across modulation rates, in an example unit (same tracker shown in **Fig. 1**). (**B**) Spike-phases relative to alpha (8 – 12 Hz) band LFPs. Note that the spikes here are the same spikes as in **A**. (**C**) Distribution of spike-phase differences between two consecutive modulation frequencies, when phases were calculated relative to theta LFPs. The observed distribution is shown in blue, whereas a surrogate (randomized differences across not-ordered modulation rates) distribution is shown in gray. There were no significant differences between the randomized and the observed distribution (Fisher's circular mean test, p = 0.38). (**D**) Same conventions as in **C**, but spike-phases were calculated relative to alpha-band LFPs. No significant differences occurred between the observed and the surrogate phase difference distributions (Fisher's circular mean test, p = 0.85). (**E**) Histogram (top) and circular histogram (bottom) for the distribution of preferred spike-phases (relative to theta-band LFPs) in tracking units (n = 31), across all modulation frequencies tested (i.e. each tracking unit and modulation frequency is represented). The red trace in the top histogram illustrates the phase convention relative to the LFP; the red line in the circular histogram shows the mean vector of the phase distribution. Statistics showed that there was a significant directionality in the spike-phases (Rayleigh test for non-uniformity, $p = 6.80 \times 10^{-67}$). (**F**) Same as conventions than panel **E**, but spike-phases were calculated relative to alpha-band LFPs. There was a significant directionality in the spike-phases relative to the alpha oscillations ($p = 1.52 \times 10^{-30}$).

Transparent Methods

Surgical procedures and animal preparation

All experimental procedures were in compliance with current German laws on animal experimentation, and were approved by the Regierungspräsidium Darmstadt (experimental permit #FU-1126). The study was performed on 7 fruit eating bats *Carollia perspicillata* (3 males). Animals were obtained from the colony in the Institute for Cell Biology and Neuroscience of the Goethe University in Frankfurt am Main, Germany.

Before undergoing surgery, the animals were subcutaneously anesthetized with a mixture of ketamine (10 mg * kg^{-1} Ketavet, Pfizer) and xylazine (38 mg * kg^{-1} Rompun, Bayer). Local anesthesia (ropivacaine hydrochloride, 2 mg/ml, Fresenius Kabi, Germany) was subcutaneously applied in the area of the scalp prior to surgery and to any subsequent handling of the wounds. A longitudinal midline incision was made along the skin covering the superior part of the head. Skin and muscle tissues were removed to expose the skull around the region of interest (the AC), such that sufficient area of the bone would remain uncovered to place a custom-made metal rod (1 cm length, 0.1 cm diameter), used to fix the head of the bat during the experimental sessions. The metal rod was attached to the skull using dental cement (Paladur, Heraeus Kulzer GmbH, Germany).

The location of the auditory cortex was determined macroscopically with the aid of previously described landmarks (Esser and Eiermann, 1999; Hechavarria et al., 2016), such as the pseudocentral sulcus and prominent blood vessels in its vicinity. Once located, the AC was exposed by cutting a small hole (roughly of 1 mm^2) in the skull with the aid of a scalpel blade. After surgery, the animals were allowed to rest for at least 2 days before being used for the electrophysiology measurements.

Neuronal recordings were performed chronically in awake bats (no anesthetic was applied on the day of the recording sessions). The experimental sessions lasted for no more than 4 h a day. During recordings, water was offered to the animal at periods of 1 – 1.5 hr. Each bat had at least one day of recovery after each session, and was not used for more than 6 experiments altogether.

Electrophysiological recordings

Experiments were conducted inside a sound-proofed and electrically shielded chamber containing a custom-made holder in which the bat was placed during measurements. The temperature of the holder was kept constant by means of an underlying heating blanket set to

30°C (Harvard, Homeothermic blanket control unit). The speaker (NeoCD 1.0 Ribbon Tweeter; Fountek Electronics, China) used for free-field stimulation was placed inside the chamber, 12 cm away from the bat's right ear, contralateral to the AC in the left hemisphere where recordings were performed. The speaker was calibrated using a $\frac{1}{4}$-inch microphone (Brüel & Kjaer, model 4135, Denmark) connected to a custom-made microphone amplifier.

Electrophysiological data was acquired by inserting a carbon electrode (Carbostar-1, Kation scientific; Impedance at 1 kHz: 0.4 – 1.2 MΩ) into the AC of the left hemisphere of the bat. A silver wire, touching the dura of a non-auditory area of the contralateral hemisphere, was used as reference electrode. The depth of the carbon electrode was accurately controlled from outside of the chamber with a Piezo manipulator (PM-101, Science products GmbH, Hofheim, Germany). Recordings were performed at depths between 300-500 µm from the cortical surface, corresponding to layers III/IV of the primary auditory cortex (AI), although we cannot discard the presence of neurons from the high frequency fields (Esser and Eiermann, 1999). Electrical signals were amplified (Dagan EX4-400 Quad Differential Amplifier, Minneapolis, MN; gain = 100, filter low cutoff frequency = 0.01 Hz, high cutoff frequency = 3 kHz), and underwent an analog-to-digital conversion (RP2.1 Enhanced real time processor, Tucker-Davies Technologies, 2 channel A/D converter, 2 channel D/A converter, 24-bit precision, Alachua, FL) with a sampling rate of 12.2 kHz before being sent to the recording computer via USB, in which the data was stored and online monitored with a custom-written Matlab (version 7.9.0.529 (R2009b), MathWorks, Natick, MA) software.

Acoustic stimulation

Acoustic stimulation was controlled with the custom-written Matlab software that was used for electrophysiological data acquisition (see above). Frequency-level receptive fields were calculated from responses to pure-tone stimuli with a duration of 10 ms (0.5 ms rise/fall time), with randomly selected frequencies ranging from 5 to 90 kHz (5 kHz steps), and sound pressure levels (SPL) from 20 to 80 dB SPL (steps of 10 dB SPL). The SPL of the tones was adjusted online according to the calibration curve of the stimulation speaker, and each frequency-level combination was repeated 5 to 8 times. Based on the frequency receptive fields of the recorded units, it was possible to define a best frequency (BF) / best level (BL) combination to which the unit was most responsive (i.e. the unit fired the highest number of spikes across all pure-tones tested). The BF/BL combination of each unit was used for synthetizing the AM sounds (see below).

Sinusoidally amplitude modulated sounds were generated by multiplying a carrier sinusoid with other slower (modulating) sinusoidal signal. The frequency of the carrier was adjusted to the BF of the unit that was being analyzed, and the SPL of the stimulus was set to be equal to the unit's BL. Modulation frequencies ranged from 2 – 157.59 Hz, increasing in an exponential manner and comprising the following 10 values: 2, 3.25, 5.28, 8.57, 13.92, 22.63, 36.76, 59.71, 97 and 157.59 Hz, with a modulation index of 1. The duration of the AM sounds was set to 1 s, and a linear fading function (10 ms in length, varying from 0 to 1) was multiplied to the beginning and the end of each acoustic stimulus to avoid artefacts during sound presentation. Each AM stimulus was presented for at least 20 repetitions in a randomized order, with a 500 ms inter-stimulus interval, and a pretime per trial (i.e. time lapse between the start of the recording and the stimulus onset) of 10 ms.

All generated sounds were converted to analog signals with a sound card (M2Tech Hi-face DAC, 384 kHz, 32 bit) prior presentation, and sent to an analog power amplifier (Rotel power amplifier, model RB-1050) in order to be presented to the bat through the speaker located inside the chamber (see above for specifications).

Separation of spikes and LFPs

All data analyses were performed off-line with custom-written Matlab (version 8.6.0.267246 (R2015b)) scripts. Spikes and LFPs were separated by digitally filtering the acquired raw signal with a 3rd order band-pass Butterworth filter with cutoff frequencies of 0.1 and 300 Hz for LFPs, and of 300 to 3000 Hz for spikes. Spike detection was based on their amplitude relative to the recording noise baseline, and spike threshold was defined manually for each unit. The spike pattern obtained in response to AM sounds was visualized by means of raster plots and peri-stimulus time histograms (PSTHs) with 1 ms bins.

Trials with motion artefacts were identified offline by looking for large 'pseudo-spikes'. Such pseudo-spikes occurred in long bursts and were higher in amplitude than 'real' spikes. We observed that the set of spike amplitudes in the recorded units followed a gamma-like distribution. With this in mind, we defined a threshold for 'pseudo-spiking events' at the 8th decile (i.e. 80% of the values) of the spike amplitude distribution for a particular unit (including all detected spikes). If a single trial contained more than 10 occurrences of pseudo-spiking events (that is, more than 10 spikes larger than the defined threshold in the 8th decile), such trial was considered as contaminated by motion artefacts and was not used for any subsequent analyses. Thorough visual inspection of raster plots and PSTHs corroborated that the overall response of the units was 'cleaned' of artefacts. If the method failed to 'clean' the

response, or too many trials were lost (> 50%), the unit was not considered for further analyses. In our data, the second case did not occur.

Spike – stimulus synchrony

The synchronization of the spiking activity of cortical units was quantified with the vector strength (VS) metric (Goldberg and Brown, 1969). The VS is a coefficient between 0 and 1 that indicates the strength of synchronicity, and is equivalent to the 'circular mean' of the phase distribution of the spikes relative to the stimulus envelope. It was calculated on a trial-by-trial basis for each modulation frequency, in every unit. In a single trial, the VS was defined as follows:

$$VS = \left|\frac{1}{n}\sum_{k=1}^{n} e^{i\phi_k}\right| \quad (1),$$

where n is the number of spikes fired in that trial, and ϕ_k is the phase of the *k*-th spike relative to the stimulus envelope.

In order to statistically validate the synchronization index provided by the VS values in a particular unit, we conducted a Rayleigh test by pooling all the spikes fired in all trials for every modulation frequency tested. A unit was considered as phase-locked in a certain modulation frequency if it met two criteria: (i) the p-value of the Rayleigh test was lower than 10^{-5}, and (ii) the median VS of the unit at that modulation frequency was higher than the population median in the same frequency. The combination of these criteria is referred as the "joint criterion", and was used to corroborate significant outcomes of the Rayleigh test, which might yield type I errors in specific occasions (Yin et al., 2011). If a unit did not meet the joint criterion in a certain modulation frequency, it was considered as not synchronized to that specific AM.

Additionally, we observed that independently of the modulation frequency tested, most of the units had a strong onset response (heavy burst of spiking activity), lasting up to 70 – 100 ms after stimulus presentation. Therefore, to avoid possible biases in the calculations due to the described onset response, only spikes that occurred past the time mark of 100 ms after stimulus onset were considered for analyses.

Spike – LFP coherence

The spike-field coherence (SFC; (Grasse and Moxon, 2010; Rutishauser et al., 2010)) was used to quantify the synchronization between the spiking activity and the LFP of the recorded units in response to AM sounds. Briefly described, the SFC is a frequency-dependent

coherence index that ranges between 0 and 1, indicating the degree of synchronization (0, for complete lack of synchrony; 1, for perfect synchrony) between action potentials and LFPs.

Conceptually, the method is based on the selection of a number of LFP windows from a longer LFP trace. LFP windows are selected at the times of spike occurrences in a particular neuron. The mean of these windows is termed spike-triggered average (STA). Because of the averaging, the STA maintains only those oscillatory components that are phase-consistent among the considered LFP segments and thus phase-consistent with the spike timings, whereas non-phasic LFP components are 'averaged out'. For calculating the SFC, the power of the STA is normalized by the average of the power spectrum obtained from each individual LFP window analysed. The latter is known as the spike-triggered power (STP). The ratio between the power of the STA and the STP yields a coefficient between 0 and 1 that describes the strength of synchrony depending on the frequency. The SFC can be expressed as follows:

$$SFC(f) = \frac{\Psi(\mathrm{STA})}{\frac{1}{n}\sum_{i=1}^{n}\Psi(w_i)} \qquad (2),$$

where $\Psi(\cdot)$ is the function used for obtaining the power spectrum, and the denominator is the STP of a series of LFP windows $w_{1,2,3,\ldots,n}$. The spectrum obtained when calculating coherence values is referred to as coherence spectrum.

Because the SFC metric is sensitive to the number of spikes used for its calculation (Grasse and Moxon, 2010), we used only those units that fired a minimum of 40 spikes in response to each modulation frequency tested. Since individual trials in our data were unlikely to contain that amount of spikes, we pooled the spikes belonging to all the trials of the same modulation frequency tested in a particular unit, and selected randomly 40 of them to use as centers for the LFP windows. Note that this implies that if there is consistent phase coherence between spikes and LFPs, it will be maintained across trials. The random selection of 40 spikes was repeated 300 times in order to reduce sampling effects, yielding an equal number (300) of SFC curves for each unit and modulation frequency. The median of these curves was considered as the SFC in the modulation frequency for the unit under consideration.

The LFP windows used for SFC computations were chosen to spread $\pm$ 200 ms from the time of spike occurrence, and only spikes for which their windows' edges fit in the time lapse of 100-1000 ms after stimulus onset were considered. The power spectra of the LFP segments were obtained with the multitaper method (Percival and Walden, 1993), available in the Chronux toolbox (Bokil et al., 2010), using 2 tapers with a time-bandwith (TW) product of 2. All power spectra in the manuscript were calculated with the same parameters.

To compare values of SFC against those that would occur by chance, we calculated a reference baseline by destroying spike-related phase synchrony across LFP segments chosen from trials belonging to a specific modulation frequency. The baseline was constructed by selecting 40 LFP windows (same number of segments used to calculate the SFC) centered at random time points, such that the windows' edges were not more extreme than times of 100 or 1000 ms after stimulus onset (same as above). The same analyses used for computing the SFC (see preceding text) were applied to these windows, yielding a baseline SFC in which values of phase coherence for this unit were disassociated from actual spike times. This procedure was repeated 300 times, rendering the same number of baseline SFC curves. Note that the same window length, number, and spectral analysis used for obtaining the SFC were used to obtain the baseline. In the manuscript, we refer to the averaged LFP windows used for baseline calculations as random-triggered average (RTA), to the average power of such windows as the random-triggered power (RTP), and to the corresponding field coherence as random-field coherence (RFC). This nomenclature was defined in a way that relates to terms such as STA, STP, and SFC, while still allowing to differentiate spike-centered and randomized coherence metrics.

The median SFC value of each unit, across modulation frequencies, was z-normalized to the corresponding RFC (i.e. the baseline distribution of SFC values). The z-normalized SFC was used to compare statistically coherence values between tracking and non-tracking units. Statistics were performed comparing the mean z-normalized SFC in canonical LFP bands (theta, 4 - 8 Hz; alpha ,8 – 12 Hz; low beta, 12 – 20 Hz; and high beta, 20 – 30 Hz), between tracking and non-tracking units, with FDR-corrected (Benjamini and Hochberg procedure; (Benjamini and Hochberg, 1995)) non-parametric Wilcoxon ranksum tests.

LFP – stimulus coherence

To address the synchronization between LFPs and the stimulus' envelope we extended the SFC approach into a slightly different metric: the stimulus-field coherence (StimFC). The principle behind this metric is clearer when considering the envelopes of the presented AM sounds as well defined periodic and phasic events. With this in mind, it is possible to quantify the phase-locking of the LFP to the stimulus' envelope by selecting a series of windows, each related to the same time point (i.e. a particular trough, a valley, or any desired phase of the envelope), across test trials of the same modulation frequency. The average of these windows is then the stimulus-triggered average (StimTA), and the mean power spectrum would be the stimulus-triggered power (StimTP). Note that, as it occurs with the STAs, only phase-

consistent oscillatory events will remain after the averaging is performed. Similar to the SFC, the StimFC is calculated as follows:

$$StimFC(f) = \frac{\Psi(\,\mathrm{StimTA}\,)}{\frac{1}{n}\sum_{i=1}^{n}\Psi(\,w_i\,)} \quad (3),$$

where the symbols indicate the analogous values to eq. (2). The only difference is that for the StimFC calculation, LFP windows are not chosen around spike times, but related to a particular time point of interest relative to the stimulus onset.

The nature of the approach makes the StimFC metric sensitive to the number of windows used. To quantify coherence between LFP and stimulus' envelopes across modulation frequencies, we sacrificed unit specificity in order to bring power to the method by increasing the amount of considered windows. Per modulation frequency, a total of 300 LFP segments (900 ms long) starting at 100 ms after stimulus onset, were randomly chosen from a pool that included all the trials from the units tested in the modulation frequency of interest (either tracking units or non-tracking units at once). Although unit specificity was lost, this approach allowed us to address whether the non-simultaneously recorded LFPs in different sites of the auditory cortex (across electrode penetrations), and even different animals, still exhibited some degree of synchronization related to the stimulus envelope. Note that after averaging across units and trials, synchronized oscillatory patterns will appear only if they are triggered by (and related to) the stimulus, while being independent of the unit they were related to, or the animal from where they came. The selection of 300 random segments was repeated 500 times, and each StimFC curve was used for further comparisons.

In a similar manner, baseline StimFC values were computed per modulation frequency by randomly selecting LFP windows (n = 300, spanning 100 – 1000 ms after stimulus onset; 500 repetitions) from the same 'pooled' trials that were used for the StimFC calculations. However, each selected window was split at a random time point, and the resulting parts of the LFP segment were swapped. Note that this effectively destroys phase consistencies between the segments and the AM envelope, and thus allows to calculate surrogate coherence estimates. As with the SFC analyses (see above), observed StimFC values were z-normalized to such surrogate StimFC, on a modulation rate basis.

Modulation of the low-frequency LFP amplitude by the stimulus phase

Phase-amplitude coupling (PAC) analyses were performed as described in (Tort et al., 2010). We focused on the modulation of the amplitude of low-frequency LFPs by the phase of the

stimulus' envelope, mainly because SFC differences were observed in the theta-alpha range. For this, LFPs were filtered in the canonical low-frequency bands (theta, alpha, low beta, and high beta) and their instantaneous energy $A(t)$ was calculated by means of the absolute value of the Hilbert transform. The phase component used for the PAC calculations was obtained from the stimulus envelope. The instantaneous phase $\phi(t)$ of the stimulus was readily available since it was an artificially generated AM sound. With both the instantaneous stimulus phase and LFP energy, we defined a composite time series $[\phi(t), A(t)]$, which relates the amplitude of the LFPs to each phase of the envelope. We then binned the phases into 36 equi-populated bins (10° bin size) and defined for each bin *j* a value equal to the mean LFP instantaneous energy, $A(t)$, for phases that fell within that particular bin. The amplitude of each bin was later normalized dividing the value of each bin by the sum of the values across all bins, which results in a distribution that holds the properties of a discrete probability density function (pdf). This is referred to as the "amplitude distribution" (Tort et al., 2010).

A Modulation Index (MI) was calculated by contrasting the observed amplitude distribution across phases with a random uniform (null) distribution. In this case, such null distribution reflects what would occur if the fluctuations of power in a certain LFP band would not be related to the phase of the stimulus. The MI quantifies how different the observed amplitude distribution and the null distribution are by normalizing the Kullback-Leibler (KL) distance (Kullback and Leibler, 1951), thus yielding values between 0 and 1 (0, no modulation; 1, perfect modulation). The MI was calculated as follows:

$$MI = \frac{D_{KL}(P,U)}{\log_2 N} \qquad (6)$$

where $D_{KL}(P,\ U)$ is the KL distance between the amplitude distribution (P) and the null distribution (U), and N stands for the number of bins. In order to obtain a uniform distribution, we generated 10000 uniformly distributed random numbers ranging from 1 to 36 (the number of bins used), and counted how many times a particular bin appeared in the list of random numbers. MIs were calculated for both tracking and non-tracking units (always using the same null distribution), and were then compared across modulation frequencies via non-parametric Wilcoxon ranksum tests. Statistical significance was accepted for p-values below an FDR-corrected (Benjamini and Hochberg procedure) threshold. Note that to avoid possible biases caused by onset responses, analyses were performed on envelope segments starting at the first trough past 100 ms after stimulus onset.

Inter-trial coherence

The consistency of the instantaneous phase of low frequency LFPs across trials was quantified by calculating the inter-trial coherence (ITC) metric. For each unit and modulation frequency, LFP traces were filtered according to the frequency band under consideration (4th order Butterworth filter), and their instantaneous phase was extracted by means of the Hilbert transform. Let $\phi(k,t)$ be the instantaneous phase of the filtered LFP at time *t* and trial *k*, of a particular unit in response to a certain modulation frequency. The ITC at time point *t* can be calculated according to:

$$ITC(t) = \left|\frac{1}{N}\sum_{k=1}^{N} e^{i\phi(k,t)}\right| \quad (7),$$

where N represents the number of trials. The ITC ranges between 0 and 1, indicating the strength of the phase consistency of the LFP across trials.

ITC values corresponding to the subpopulations of tracking and non-tracking units were compared across modulation frequencies, by subtracting the median ITC of the subpopulation of trackers minus the median ITC of the subpopulation of non-trackers, for every modulation rate tested. Throughout the text, we refer to this difference as the ITC difference (dITC). A surrogate dITC was generated by randomly permuting labels ("trackers", "non-trackers") of units, and recalculating the same differences between randomly labeled subpopulations, for each modulation frequency. This randomization procedure was repeated 2500 times, yielding a surrogate distribution of differences at each modulation rate, in which the actual differences between neuronal groups were minimized to chance level. Because of the large number of repetitions, for computational purposes the ITC data was down-sampled from 12.2 kHz (sampling frequency of the recording device) to 200 Hz. The dITC was z- normalized to the surrogate distribution, and the z-normalized values were used as a measure of significance, with an uncorrected threshold set at z = 1.96 (equivalent to a p-value of 0.05). Positive z-normalized dITC values indicate higher ITC in trackers than non-trackers, while negative values indicate the opposite.

Relationship between spiking, phase of the AM stimuli, and low-frequency LFPs

In order to explore the phase relation between neuronal firing and AM stimuli in the recorded units, a phase related to the AM envelope was assigned to each spike in the same way as it was done for VS calculations. As mentioned in the preceding text, spikes were only considered when they occurred in the time window between 100-1000 ms after stimulus presentation, thus avoiding onset and offset responses that could bias the calculations. The

distributions of stimulus phases at which the units fired their spikes were plotted as circular histograms for each modulation frequency. Preferred stimulus phases were obtained by calculating the phase of the mean orientation vector of the circular distribution in each unit and modulation frequency. Units were only considered for the preferred phase calculations if they fulfilled the joint criterion for the particular AM frequency under study (note that this implies that only trackers were used). The preferred AM phase of the units was studied only for the six slowest AM frequencies tested (i.e. from 2 to 22.63 Hz), as those are the frequencies most cortical neurons are capable of locking their spikes to (Martin et al., 2017).

To test for differences in the preferred phase, across modulation frequencies, the angular difference between mean orientation vectors obtained from two distinct modulation rates was calculated based on trigonometric relationships relying on the cross and the dot products between the vectors, considering that:

$$tan\phi = \frac{sen\phi}{cos\phi} = \frac{||u \times v||}{u \cdot v} \qquad (8),$$

where ϕ is the angle between vectors *u* and *v*, and $||u \times v||$ indicates the norm of the cross product between these vectors, while $u \cdot v$ stands for the dot product between them. The angle ϕ is measured in the counterclockwise direction, and a positive sign indicates a counterclockwise rotation from *u* to *v*, with an equivalent angle. In this case, vectors *u* and *v* can be thought as the mean vectors of two different modulation rates.

The effect of raising the modulation frequencies on the spike phase was quantified by calculating angular differences within each unit, between the phase of the mean orientation vectors obtained in response to two successive AM rates (a lower and a higher rate). The above was only done for pairs of modulation frequencies to which the unit was significantly synchronized, according to the joint criterion (modulation rates were chosen in such way that their values would be as close as possible). The set of differences obtained would be centered at zero, if overall the units would not change preferred phases as the presented envelopes increased in frequency. On the other hand, a shift towards positive phase differences would indicate a phase lag (the units tend to respond to a later envelope phase as modulation frequencies increase), whereas a shift towards negative phase differences would suggest a phase acceleration (the units tend to respond to an earlier phase of higher AM envelopes).

To assess statistically the presence of an effect caused by an increase of the stimulus modulation frequency, a randomization test was performed to generate a null distribution testing the hypothesis that the increase in the stimulus modulation rate does not account for

the observed distribution of phase differences. For each unit, mean vectors calculated in response to different modulation rates were randomly paired (if the unit satisfied the joint criterion in those modulation rates), and their angular difference was obtained. Such a procedure was repeated 10000 times, and the surrogate distribution carrying no effect of orderly increasing the modulation frequencies was statistically compared with the observed distribution using a nonparametric circular test for equal medians (Fisher's circular median test, threshold of $p = 0.05$).

We performed similar analyses to test whether the change in modulation frequency would affect predictably the synchronization of the spikes and the low frequency LFP bands. For each unit, we obtained the preferred spike-phase relative to low frequency LFPs (in the bands of 4 – 8, 8 – 12, or 4 - 12 Hz; 4^{th} order Butterworth filter), only considering modulation frequencies in which the unit satisfied the joint synchronization criterion. The instantaneous phase of the LFP was calculated from the Hilbert-transformed low frequency LFP.

Phase differences were obtained as described for the preferred AM phases (see preceding text), across (ordered) modulation rates. As mentioned above, a phase difference distribution centered at 0 degrees, shifted towards positive angles, or shifted towards negative angles, would indicate no phase change, a phase lag, or a phase acceleration, respectively. A randomization test similar to the one described in the preceding text was used to generate a surrogate distribution of phase differences, in which there was no effect of changing the modulation rate of the stimulus in an orderly manner (i.e. increasingly or decreasingly). The observed and randomized distributions were then statistically compared by means of a Fisher's circular median test (significance threshold at $p = 0.05$).

Supplementary references:

Benjamini, Y., and Hochberg, Y. (1995). Controlling the False Discovery Rate - a Practical and Powerful Approach to Multiple Testing. J Roy Stat Soc B Met *57*, 289-300.

Bokil, H., Andrews, P., Kulkarni, J.E., Mehta, S., and Mitra, P.P. (2010). Chronux: a platform for analyzing neural signals. Journal of neuroscience methods *192*, 146-151.

Esser, K.H., and Eiermann, A. (1999). Tonotopic organization and parcellation of auditory cortex in the FM-bat Carollia perspicillata. Eur J Neurosci *11*, 3669-3682.

Goldberg, J.M., and Brown, P.B. (1969). Response of binaural neurons of dog superior olivary complex to dichotic tonal stimuli: some physiological mechanisms of sound localization. J Neurophysiol *32*, 613-636.

Grasse, D.W., and Moxon, K.A. (2010). Correcting the bias of spike field coherence estimators due to a finite number of spikes. J Neurophysiol *104*, 548-558.

Hagemann, C., Esser, K.H., and Kossl, M. (2010). Chronotopically organized target-distance map in the auditory cortex of the short-tailed fruit bat. J Neurophysiol *103*, 322-333.

Hagemann, C., Vater, M., and Kossl, M. (2011). Comparison of properties of cortical echo delay-tuning in the short-tailed fruit bat and the mustached bat. J Comp Physiol A Neuroethol Sens Neural Behav Physiol *197*, 605-613.

Hechavarria, J.C., Beetz, M.J., Macias, S., and Kossl, M. (2016). Vocal sequences suppress spiking in the bat auditory cortex while evoking concomitant steady-state local field potentials. Sci Rep *6*, 39226.

Kullback, S., and Leibler, R.A. (1951). On Information and Sufficiency. Ann Math Stat *22*, 79-86.

Martin, L.M., Garcia-Rosales, F., Beetz, M.J., and Hechavarria, J.C. (2017). Processing of temporally patterned sounds in the auditory cortex of Seba's short-tailed bat,Carollia perspicillata. Eur J Neurosci *46*, 2365-2379.

Percival, D.B., and Walden, A.T. (1993). Spectral analysis for physical applications (cambridge university press).

Rutishauser, U., Ross, I.B., Mamelak, A.N., and Schuman, E.M. (2010). Human memory strength is predicted by theta-frequency phase-locking of single neurons. Nature *464*, 903-907.

Tort, A.B., Komorowski, R., Eichenbaum, H., and Kopell, N. (2010). Measuring phase-amplitude coupling between neuronal oscillations of different frequencies. J Neurophysiol *104*, 1195-1210.

Yin, P.B., Johnson, J.S., O'Connor, K.N., and Sutter, M.L. (2011). Coding of Amplitude Modulation in Primary Auditory Cortex. Journal of Neurophysiology *105*, 582-600.